A supramolecular bifunctional iridium photoaminocatalyst for the enantioselective alkylation of aldehydes

Andrea Gualandi, Francesco Calogero, Ada Martinelli, Arianna Quintavalla, Marianna Marchini, Paola Ceroni, Marco Lombardo and Pier Giorgio Cozzi

Dalton Trans., ***2020***, *49,* 14497-14505.

A Supramolecular Iridium Bifunctional Photoaminocatalyst for the Enantioselective Alkylation of Aldehydes

Andrea Gualandi,* Francesco Calogero, Ada Martinelli, Arianna Quintavalla, Marianna Marchini, Paola Ceroni,* Marco Lombardo* and Pier Giorgio Cozzi*

The construction of a hybrid metal-organo-photoredox catalyst based on the conjugation of an imidazolidinone organocatalyst and an $Ir(ppy)_2(bipy)$ (ppy = 2-phenylpyridine, bipy = bipyridine) is described. The introduction of the desired organocatalyst into the bipyridine moiety is quite modular, allowing the preparation of different hybrid photocatalysts, and is realized though a simple click reaction. The hybrid photocatalysts obtained were employed in the benchmark photoredox alkylation of aldehydes. Remarkably, the conjugation of a first-generation MacMillan catalyst is producing an active and stereoselective hybrid photoredox catalyst.

Introduction

In recent years photoredox catalysis has become a hot topic in modern organic synthesis.[1] Photoredox catalysis has found important applications, both in academic[2] and industrial contexts[3] leading to important developments, particularly regarding the generation of radical intermediates[4] and their employment in catalytic transformation. Formation of radicals[5] by photoredox catalysis or by different methodologies[6] can now be considered for "a radical retrosynthetic analysis".[7] The rebirth of photoredox catalysis and its rapid advancements were related principally to the use of transition metal complexes, such as ruthenium[8] or iridium complexes,[9] both capable to absorb visible light and to initiate a chemical reaction through electron or energy transfer processes from their more reactive photoexcited states.[10] The benchmark stereocontrolled organocatalytic photoredox reaction developed by MacMillan[11] started to attract the interest in the field of photoredox catalysis, and it is still used for testing new compounds as active photocatalysts.[12] In 2008, MacMillan developed a pioneering and outstanding example of synergistic catalytic system[13] in which the photoredox catalyst $Ru(bpy)_3^{2+}$ and an imidazolidinone organocatalyst were employed in the challenging organocatalytic α-alkylation of aldehydes.[14] The asymmetric α-alkylation of aldehydes and ketones has become rapidly an attractive topic for the synergistic photoredox catalysis, and diverse dual catalytic systems based on other photocatalysts (metal complexes,[15] semiconductors,[16] organic dyes[17]) were developed. It is also worth mentioning that the chiral enamine, transiently formed during the catalytic cycle, can behave as effective photocatalyst able to promote the α-alkylation of aldehydes.[18] However, nucleophilicity of enamines[19] seems to be relevant in these applications, and as imidazolidinones are forming less nucleophilic enamines,[20] the possibility to employ these organocatalysts without the presence of an active photocatalyst was not demonstrated yet. The α-alkylation of aldehydes promoted by chiral imidazolidinones is not a trivial process and there are difficulties related to the preparation of the active imidazolidinone catalyst. First generation of imidazolidinone catalysts[21] generally display poor reactivity under photoredox conditions. Furthermore, the appropriate set-up for the compatibility of two different catalytic systems (i.e. photoredox and organocatalytic cycle) need to be finely tuned. Recently, Alemán reported the development of a general photo-organocatalyst for the α-alkylation of aldehydes.[22] He reported the design of an effective bifunctional photoaminocatalyst, capable of performing the photoredox process and forming the active enamine intermediate simultaneously.

Herein, we report a full account of our studies focused on the preparation and properties of active iridium bifunctional photocatalysts. Additionally, a preliminary study on their potential applications has been carried out, using the α-alkylation of aldehydes as a benchmark reaction. For the design of the new iridium photoaminocatalysts, we have considered various issues. As primary instance, we have incorporated into a long-lived excited state iridium photocatalyst various chiral scaffolds able to form reactive enamines. Secondly, we have selected a facile system for the conjugation of an amino-organocatalyst and the metal based photocatalyst in the same supramolecular system in order to guarantee a versatile and modular approach that can be further tuned. The bifunctional photoaminocatalysts obtained were tested in the benchmark reaction of α-alkylation of aldehydes. In addition, photophysical data were also collected to support the reaction mechanism.

Experimental

Materials and methods

All commercial chemicals and dry solvents were purchased from Sigma Aldrich, Alfa Aesar or TCI Chemicals and used without additional purifications. ^1H and ^{13}C NMR spectra were recorded on a Varian Inova 400 NMR instrument with a 5 mm probe. All chemical shifts (δ) are referenced using deuterated solvent signals; chemical shifts are reported in ppm from TMS and coupling constants (*J*) are reported in Hertz. Multiplicity is reported as: s = singlet, d = doublet, t = triplet, q = quartet, hept = heptet, m = multiplet). HPLC-MS analyses were performed on an Agilent Technologies HP1100

instrument coupled with an Agilent Technologies MSD1100 single-quadrupole mass spectrometer using a Phenomenex Gemini C18 3 µm (100 x 3 mm) column; mass spectrometric detection was performed in full-scan mode from *m*/*z* 50 to 2500, scan time 0.1 s in positive ion mode, ESI spray voltage 4500 V, nitrogen gas 35 psi, drying gas flow rate 11.5 mL min^{-1}, fragmentor voltage 30 V. HRMS were performed on Waters Xevo G2-XS QTof, ESI+, cone voltage 40 V, Capillary 3 KV, source temperature 120 °C. CSP-HPLC analyses were performed on an Agilent Technologies Series 1200 instrument using chiral columns. The enantiomeric compositions were checked against the corresponding racemic products. Flash chromatography purifications were carried out using VWR or Merck silica gel (40-63 µm particle size). Thin-layer chromatography was performed on Merck 60 F254 plates.

***tert*-Butyl-(2S,3R)-3-(hex-5-yn-1-yloxy)-2-tritylpyrrolidine-1-carboxylate (N-Boc-2c)**

NaH (3 mmol, 0.12 g, 60 % in mineral oil) is added to a solution of *tert*-butyl (2*S*,3*R*)-3-hydroxy-2-tritylpyrrolidine-1-carboxylate (1 mmol, 0.43 g)[23] in DMF (5 mL) at 0 °C and the reaction mixture is stirred at 0 °C for 1 h. 6-Iodo-hex-1-yne (3 mmol, 0.4 mL) is added dropwise at 0 °C and the reaction mixture in stirred at room temperature for 18 h. The reaction was quenched with aqueous NH_4Cl, diluted with ethyl acetate and the organic phase was washed with aqueous 5% LiCl. The organic phase was dried (Na_2SO_4), concentrated under vacuum and the crude mixture was purified by flash-chromatography on silica (cyclohexane/ethyl acetate 9/1), affording *N*-Boc-**2c** as a gummy solid (0.155 g, 0.3 mmol, 30 %). ^{1}H NMR (400 MHz, $CDCl_3$) δ 7.51–7.39 (m, 6 H), 7.29–7.08 (m, 9 H), 5.81 (s, 1 H), 3.91 (d, *J* = 5.2 Hz, 1 H), 3.41 (m, 2 H), 3.22 (m, 1 H), 2.89 (td, *J* = 10.6, 2.6 Hz, 1 H), 2.27 (dt, *J* = 6.7, 3.2 Hz, 2 H), 1.96 (t, *J* = 2.6 Hz, 1 H), 1.71 (m, 4 H), 1.48–1.38 (ddd, *J* = 14.0, 10.2, 2.9 Hz 1 H), 1.34 (s, 9 H), −0.12–0.30 (m, 1 H). ^{13}C NMR (100 MHz, $CDCl_3$) δ 157.2, 144.8, 130.7, 127.3, 125.9, 84.3, 83.7, 71.2, 68.4, 67.2, 65.8, 60.9, 49.5, 28.9, 28.2, 26.7, 25.5, 18.2. $[\alpha]_D^{25}$= −80.1 (c = 0.24, $CHCl_3$). HPLC-MS (ESI): 532 [M + Na^+] 454 [M − *t*Bu + 2H^+] 1042 [2M + H^+ + Na^+]. Calcd. for ($C_{34}H_{39}NO_3$: 509.69): C, 80.12; H, 7.71; N, 2.75; found: C, 79.75, H, 7.69; N, 2.74.

(2S,3R)-3-(hex-5-yn-1-yloxy)-2-tritylpyrrolidine (2c)

Trifluoroacetic acid (20 mmol, 1.53 mL,) was added to a solution of *N*-Boc-**2c** (1 mmol, 0.51 g) in DCM (2 mL) and the reaction mixture was stirred at room temperature for 18 h. The organic solvents were removed under vacuum, the solid residue was diluted with ethyl acetate and treated with aqueous $NaHCO_3$. The aqueous phase was extracted with ethyl acetate (3 × 5 mL), the combined organic phases were dried (Na_2SO_4) and evaporated under vacuum to give pure **2c** as a gummy solid (0.37 g, 0.9 mmol, 90 %). ^{1}H NMR (400 MHz, $CDCl_3$) δ 7.40 (d, *J* = 7.6 Hz, 6 H), 7.29–7.12 (m, 9 H), 4.84 (s, 1 H), 3.63 (d, *J* = 5.0 Hz, 1 H), 3.45 (dtd, *J* = 8.8, 6.4, 5.6, 3.2 Hz, 1 H), 3.15 (dt, *J* = 8.1, 5.5 Hz, 1 H), 2.93 (ddd, *J* = 11.8, 9.0, 5.4 Hz, 1 H), 2.75 (t, *J* = 8.2 Hz, 1 H), 2.27 (hept, *J* = 2.6 Hz, 2 H), 1.98 (t, *J* = 2.6 Hz, 1 H), 1.81–1.64 (m, 5 H), 1.53 (dd, *J* = 13.1, 5.4 Hz, 1 H), 0.29 (tdd, *J* = 12.6, 7.5, 5.1 Hz, 1 H). ^{13}C NMR (100 MHz, $CDCl_3$) δ 130.2, 127.5, 125.9, 84.3, 83.2, 77.3, 77.0, 76.7, 70.9, 68.5, 68.1, 60.9, 44.8, 30.2, 29.2, 25.6, 18.3, 1.0. $[\alpha]_D^{25}$= −97.16 (c = 0.33, $CHCl_3$). HPLC-MS (ESI): 410 [M + H^+]. Calcd. for ($C_{29}H_{31}NO$: 409.57): C, 85.04; H, 7.63; N, 3.42; found: C, 85.30, H, 7.66; N, 3.43.

Synthesis of catalysts 3a-c, general procedure

Tetrakis(acetonitrile)copper(I) hexafluorophosphate (0.023 mmol, 8.9 mg, 0.25 equiv.) was added to a mixture of Ir(N_3-CH_2bpy)(ppy)$_2$]PF_6[24] (**1**, 83.1 mg, 0.095 mmol) and the desired organocatalyst (**2a-c**, 0.095 mmol) in dichloromethane (0.5 mL) and the reaction mixture is stirred at room temperature for 48 h. The crude mixture was poured on top of a silica gel flash-chromatography column and directly purified by eluting first with dichloromethane and then with dichloromethane/methanol 9:1.

3a. Yellow solid, Y = 75 %. ^{1}H NMR (400 MHz, CD_3CN, two stereoisomers) δ 8.31 (d, *J* = 4.1 Hz, 1 H), 8.23 (dd, *J* = 9.2, 1.5 Hz, 1 H), 8.04 (dd, *J* = 8.3, 5.5 Hz, 2 H), 7.93 (d, *J* = 5.7 Hz, 1 H), 7.87–7.72 (m, 6 H), 7.65 (d, *J* = 1.7 Hz, 1 H), 7.62–7.51 (m, 2 H), 7.33 (d, *J* = 5.8 Hz, 1 H), 7.23–7.10 (m, 4 H), 7.09–6.95 (m, 5 H), 6.90 (tdd, *J* = 7.4, 2.4, 1.3 Hz, 2 H), 6.27 (td, *J* = 7.2, 1.3 Hz, 2 H), 5.72 (s, 2 H), 4.52 (dd, *J* = 15.8, 2.0 Hz, 1 H), 4.36 (dd, *J* = 15.8, 3.0 Hz, 1 H), 3.74 (ddd, *J* = 8.0, 4.3, 1.4 Hz, 1 H), 3.04 (ddd, *J* = 14.2, 4.2, 2.8 Hz, 1 H), 2.78 (ddd, *J* = 14.0, 7.9, 3.5 Hz, 1 H), 2.53 (s, 3 H), 1.193 and 1.186 (s, 3H), 1.15 and 1.14 (s, 3H). ^{13}C NMR (100 MHz, CD_3CN, two stereoisomers) δ 175.10 and 175.08, 168.9, 168.8, 157.91 and 157.89, 156.32 and 156.31, 153.6, 152.35 and 152.33, 151.8, 151.7, 151.4, 150.52 and 150.51, 150.54, 150.0, 147.1, 145.5, 145.4, 139.97 and 139.95, 139.8, 139.7, 133.01 and 132.91, 131.81 and 131.79, 131.00 and 130.98, 130.0, 129.62, 129.59, 127.93, 127.88, 127.80, 127.77, 126.99 and 126.97, 126.97 and 126.95, 126.33 and 126.31, 125.4, 125.0, 124.90 and 124.89, 124.14 and 124.13, 123.96 and 123.94, 121.3, 77.5, 60.23 and 60.20, 53.2, 38.92 and 38.86, 36.57 and 36.56, 29.01 and 28.99, 27.16, 21.92. HPLC-MS (ESI): 968 [M − PF_6]$^+$, 484 [2M − PF_6 + H]$^+$. HRMS (ESI/Flow Injection): Calcd for $C_{49}H_{45}IrN_9O$ 968.3376; Found 968.3379.

3b. Yellow solid, Y = 97 %. ^{1}H NMR (400 MHz, CD_3CN, two stereoisomers) δ 8.42 (s, 1 H), 8.35 (s, 1 H), 8.04 (dd, *J* = 8.1, 3.1 Hz, 2 H), 7.98 (s, 1 H), 7.92 (d, *J* = 5.7 Hz, 1 H), 7.88–7.73 (m, 5 H), 7.60 (t, *J* = 6.8 Hz, 1 H), 7.32 (d, *J* = 5.6 Hz, 1 H), 7.20 (d, *J* = 5.7 Hz, 1 H), 7.16 (d, *J* = 8.4 Hz, 2 H), 7.07–6.97 (m, 4 H), 6.94–6.84 (m, 4 H), 6.27 (dd, *J* = 6.8, 5.3 Hz, 2 H), 5.74 (s, 2 H), 5.13 (s, 2 H), 3.63 (s, 1 H), 3.02 (dd, *J* = 14.2, 3.8 Hz, 1 H), 2.72–2.61 (m, 4 H), 2.52 (s, 3 H), 1.95 (dt, *J* = 5.0, 2.5 Hz, 1 H), 1.20 (s, 6 H). ^{13}C NMR (100 MHz, CD_3CN, two stereoisomers) δ 174.3, 168.42 and 168.35, 157.9, 157.5, 155.9, 153.1, 151.9, 151.31 and 151.25, 150.9, 150.13 and 150.09, 149.1, 145.2, 145.06 and 144.98, 139.53 and 139.50, 132.55 and 132.46, 132.2, 131.4, 131.35 and 131.33, 130.3, 127.8, 126.6, 125.87 and 125.85, 125.76, 124.49 and 124.45, 124.3, 123.51 and 123.48, 120.85 and 120.83, 115.6, 76.5, 62.4, 60.4, 52.8, 37.8, 27.6, 25.5, 25.3, 21.5. HPLC-MS (ESI): 998 $[M - PF_6]^+$, 499 $[2M - PF_6 + H]^+$. HRMS (ESI/Flow Injection): Calcd for $C_{50}H_{47}IrN_9O_2$ 998.3482; Found 998.3476.

3c. Yellow solid, Y = 90 %. ^{1}H NMR (400 MHz, $CDCl_3$, two stereoisomers) δ 8.59–8.36 (m, 2 H), 7.91–7.79 (m, 4 H), 7.82–7.70 (m, 4 H), 7.70–7.60 (m, 2 H), 7.54–7.47 (m, 2 H), 7.47–7.31 (m, 6 H), 7.24–7.18 (m, 6 H), 7.18–7.12 (m, 4 H), 7.06–6.96 (m, 4 H), 6.94–6.22 (m, 2 H), 6.30–6.22 (m, 2 H), 5.76 (s, 1 H) and 4.97-4.84 (m, 1H), 4.77 (s, 1 H), 3.70–3.60 (m, 1 H), 3.46–3.73 (m, 1 H), 3.21-3.10 (m, 1 H), 3.01-2.83 (s, 1 H), 2.84-5.69 (m, 1 H), 2.58 and 2.54 (s, 3 H), 2.30-2.24 (s, 1 H), 2.00-1.96 (s, 1 H), 1.77-1.63 (m, 4 H), 1.59-1.50 (m, 1 H), 0.20-0.35 (m, 1 H). ^{13}C NMR (100 MHz, CD_3CN, two stereoisomers) δ 168.47 and 168.41, 157.4, 156.0, 153.1, 151.9, 151.29 and 151.22, 150.9, 150.1, 149.6, 145.05 and 144.99, 139.54 and 139.49, 139.51, 132.56 and 132.47, 131.4, 130.3, 128.6, 128.3, 127.7, 126.6, 125.9, 124.46 and 124.43, 123.5, 120.9, 52.7, 32.7, 30.4, 30.2, 30.0, 27.0, 26.0, 23.4, 22.3, 21.5, 19.3. HPLC-MS (ESI): 1135 $[M - PF_6]^+$, 568 $[2M - PF_6 + H]^+$. HRMS (ESI/Flow Injection): Calcd for $C_{63}H_{58}IrN_8O$ 1135.4363; Found 1135.4359.

Phototocatalytic alkylation of aldehydes, general procedure

In a Schlenk tube with rotaflo stopcock under argon atmosphere at r.t., the catalyst **3a-c** (0.005 mmol, 0.01 equiv.), a solution of trifluoromethansulfonic acid (0.1 M in DMF, 0.005 mmol, 50 µL, 0.01 equiv) and DMF (0.45 mL) were sequentially added. After 15 minutes, bromoderivatives **5a-b** (0.05 mmol), **4** (20 µL, 0.15 mmol, 3 equiv.) and 2,6-lutidine (12 µL, 0.1 mmol, 2 equiv.,) were then added. The reaction mixture was carefully degassed via freeze-pump thaw (three times), and the vessel refilled with argon. The Schlelk tube was stirred and irradiated with blue LEDs. After 24 h of irradiation, aq. HCl 1M (2 mL) was added and the mixture was extracted with AcOEt (4 x 5 mL). The organic phase was dried (Na_2SO_4), concentrated under vacuum and the crude mixture was purified by flash-chromatography on silica.

6a. The title compound was isolated by flash column chromatography (SiO_2, cyclohexane/EtOAc 95/5) as colorless oil. Y = 84%, *ee* = 60%. ee before column purification was 70%. *Ee* was determined by chiral HPLC analysis using Daicel Chiralpak®IC column: hexane/*i*-PrOH 90/10, flow rate 1.00 mL/min, 30°C, λ = 210 nm: t_{major} = 18.9 min., t_{minor} = 14.7 min.; ^{1}H NMR and ^{13}C NMR were according to those reported in literature.[11]

6b. The title compound was isolated by flash column chromatography (SiO_2, cyclohexane/EtOAc 97/3) as colorless oil. Y = 77%, *ee* = 77%. ee before column purification was 80%. *Ee* was determined by chiral HPLC analysis using Daicel Chiralpak®IC column, hexane/*i*-PrOH 90/10, flow rate 1.00 mL/min, 30°C, λ = 210 nm: t_{major} = 17.8 min., t_{minor} = 14.9 min.; ^{1}H NMR and ^{13}C NMR were according to those reported in literature.[16b]

Result and discussions

Due to the mild reaction conditions required, copper-mediated azide–alkyne cycloadditions (CuAACs) have been largely used to couple different groups onto ruthenium(II) polypyridyl-type sensitizers.[25] Inspired by a recent work on the preparation of artificial photosynthetic dendrimers,[24] we decided to bind the azido-substituted iridium photo-sensitizer (**1**) to some suitably functionalized representative organocatalysts (**2**), exploiting a click-chemistry approach. The general retrosynthetic strategy used for the preparation of iridium bifunctional photoaminocatalysts **3** through CuAAC is outlined in Scheme 1.

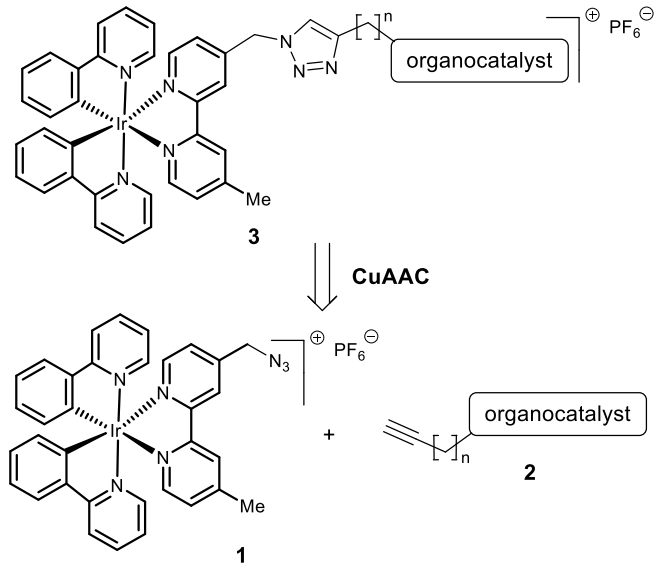

Scheme 1. Synthetic strategy for the preparation of iridium bifunctional photoaminocatalysts **3**.

Three different alkyne-functionalized organocatalysts **2a-c** were chosen as reaction partners (Figure 1). **2a** and **2b** derived from MacMillan imidazolidin-4-ones, while **2c** from Maruoka 2-triphenylmethyl pyrrolidine. CuAAC of L-phenylalanine-derived imidazolidin-4-one **2a** was recently used for the preparation of a recyclable magnetic nano-catalyst, employed in asymmetric 1,3-dipolar cycloadditions.[26] Similarly, L-tyrosine-derived imidazolidin-4-one **2b** was used to synthesize a recyclable pentaerythritol supported catalyst, exploited in enantioselective Diels–Alder reactions[27a] and in the immobilization of the catalyst on siliceous mesocellular foams.[27b] Propargylated derivative of (2*S*,3*R*)-3-hydroxy-2-triphenylmethyl-pyrrolidine was recently used by us in a CuAAC

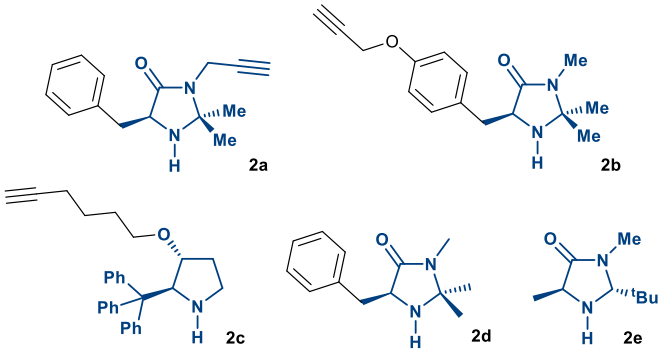

Fig. 1. Structures of organocatalysts **2a-e**.

to prepare a recyclable [60]fullerene-hybrid catalyst, employed in the enantioselective Michael addition of malonates to α,β-unsaturated aldehydes.[23] In similar manner organocatalyst **2c** was easily prepared starting from commercial 6-iodo-hex-1-yne and the same pyrrolidine. The click-chemistry reaction of **1** with **2a-c** proceeded smoothly using 25 mol% of tetrakis(acetonitrile)copper(I) hexafluorophosphate catalyst in DCM at room temperature for 48 h, allowing to obtain the desired iridium bifunctional photoaminocatalysts **3a-c** (Figure 2)

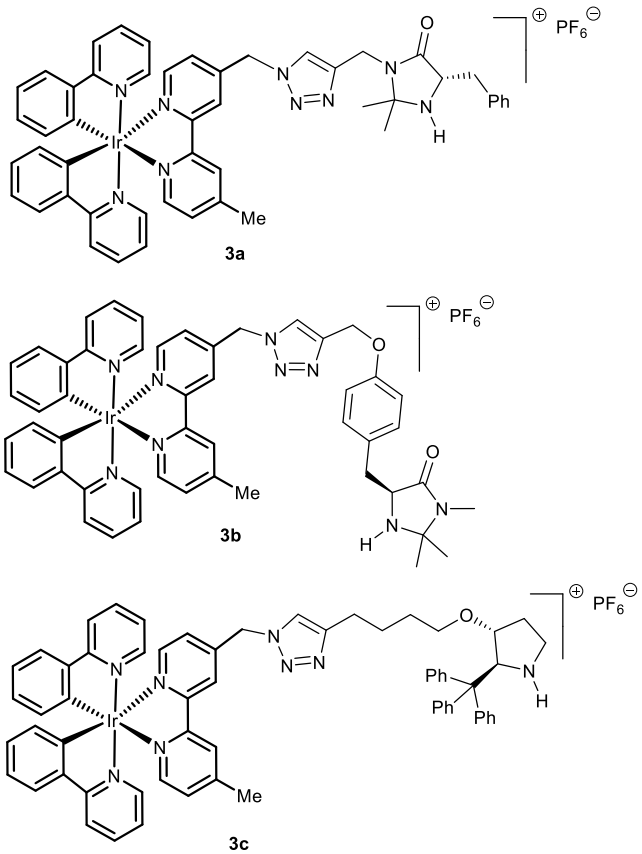

Fig. 2. Structures of iridium bifunctional photoaminocatalysts **3a-c**.

from good to very high isolated yields, after purification by flash-chromatography (**3a**: Y = 75%, **3b**: Y = 97%, **3c**: Y = 90%).

A photophysical analysis of the photocatalysts was carried out (Table 1). Absorption and emission spectra of **3a-c** are dominated by the Ir(III) complex moiety. The three photocatalysts show very similar photophysical properties both in acetonitrile (Figure 3) and DMF solution. The phosphorescence lifetime, measured in air-equilibrated DMF solution at room temperature, is ca. 110 ns for all of them (Table 1), similar to the value of 124 ns registered for the model $[Ir(ppy)_2(dtbbpy)]PF_6$ under the same experimental conditions.

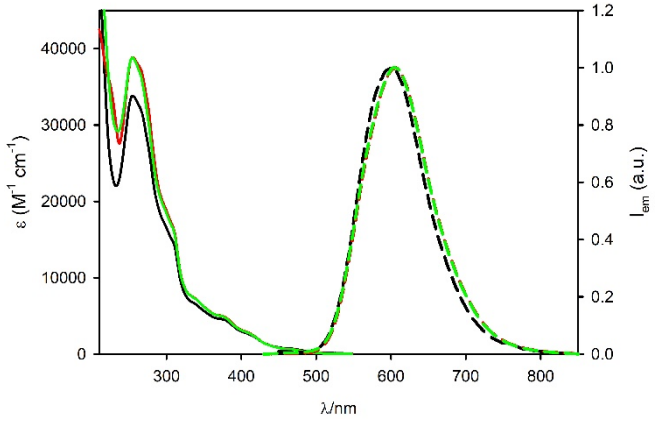

Fig. 3. Absorption and emission spectra of the photocatalysts **3a** (black solid line and dashed solid line), **3b** (red solid line and dashed line) and **3c** (green solid line and dashed line) in air-equilibrated acetonitrile solution at room temperature. λ_{ex} = 400 nm.

From the photophysical analysis (Table 1) it is evident that the functionalization of the photocatalyst with organocatalysts does not affect the photophysical properties of the metal complex, that are comparable with that of $[Ir(ppy)_2(dtbbpy)]PF_6$.

Table 1. Photophysical properties of iridium complexes **3a**-**c** in air-equilibrated acetonitrile solution, 298 K, unless otherwise noted.

	Absorption		Emission	
	λ/nm	ε/10^{-4} M^{-1} cm^{-1}	λ/nm	τ (ns)[a]
	255	3.38		
3a	311	1.41	600	108
	387	0.43		
	255	3.88		
3b	311	1.56	604	110
	387	0.45		
	255	3.89		
3c	311	1.59	606	114
	387	0.46[c]		
	257	2.53[d]		
Ir[b]	299	1.16[d]	581[d]	124
	381	0.26[d]		

[a] Value estimated in air-equilibrated DMF solution, 298 K. [b] **Ir** = $[Ir(ppy)_2(dtbbpy)]PF_6$. [c] Value from ref 28. [d] Value from ref 29.

We tested the three supramolecular photocatalysts, using the standard reaction conditions developed by MacMillan for the enantioselective α-alkylation of aldehydes (Table 2).[11]

Table 2. Photocatalytic enantioselective α-alkylation of hydrocinnamaldehyde (**4**) catalysed by **3a-c** and **2b**.

4 **5a,b** **6a,b**

a: $R^1 = CO_2Et$, $R^2 = OEt$
b: $R^1 = H$, $R^2 = Ph$

Entry[a]	Catalyst	Product	% conv.[b] (% yield)[c]	*ee*[d]
1	**3a**	**6a**	26	30
2	**3b**	**6a**	>99 (84)	70
3	**3b**[e]	**6a**	28	70
4	**3c**	**6a**	22	n.d.
5[f]	**2b**	**6a**	64 (57)	59
6[g]	**2b**	**6a**	<5	n.d.
7	**3a**	**6b**	26	57
8	**3b**	**6b**	>99 (77)	80
9	**3c**	**6b**	0	-
10[f]	**2b**	**6b**	9	n.d.

[a] Reactions were performed on 0.05 mmol of **5** in DMF (0.5 mL). [b] Determined by ^1H NMR analysis of the reaction crude using internal standard method. [c] Determined after chromatographic purification. [d] Determined by HPLC analysis on chiral stationary phase of the reaction crude. [e] The reaction was performed with 5 mol% of **3b** and TfOH. [f] 2 mol% of $[Ir(ppy)_2(dtbbpy)]PF_6$ was used as photoredox catalyst in the reaction. [g] Reaction performed in absence of $[Ir(ppy)_2(dtbbpy)]PF_6$. n.d. = not determined.

Hydrocinnamaldehyde (**4**) and bromo derivatives **5a**,**b** were chosen as model substrates. The reaction was performed under blue LEDs irradiation using DMF as solvent in the presence of 2,6-lutidine, 10 mol% of the catalyst and 10 mol% of trifluoromethansulfonic acid (TfOH) to promote the enamine formation. **3b** was the most effective catalyst, giving the alkylation products in good yields and satisfying enantiomeric excesses (Table 2, entries 2 and 8). Imidazolidinone catalyst **3a** (Table 2, entries 1 and 7), carrying the iridium complex moiety on the amide nitrogen, gave poor results in term of yield and enantioselectivity. Similar results were obtained with the pyrrolidine based catalyst **3c** (Table 2, entries 4 and 9).

The supramolecular approach, which combines the photosensitizer and the organocatalyst in the same system, resulted in a significant improvement in the catalytic performance. This is clearly evident by the comparison with the separated components, namely imidazolidinone **2b** organocatalyst and $[Ir(ppy)_2(dtbbpy)]PF_6$ photosensitizer (Table 2, entries 5 and 10). The reaction leads to the formation of the product **6a** with 57% yield and 59% *ee*, while poor results were obtained using **5b** as bromoderivative. The lower performances obtained compared to those observed with the supramolecular photocatalyst **3b** (84% yield, 70% *ee* for **6a**), demonstrates how the spatial proximity of the two functions improves the synergy of the entire process, both in terms of yield and of enantioselectivity.

To exclude that the enamine, transiently formed during the catalytic cycle, was able to promote the α-alkylation of aldehydes behaving as effective photocatalyst,[30] a test using chiral imidazolidinone **2b** in absence of iridium complex was performed (Table 2, entry 6). Only traces of product **6a** were observed after 24 h of irradiation with blue LEDs, excluding this reaction pathways.

The scarce results in terms of yield and enantioselectivity obtained with catalyst **3a** could be attributed to the presence of the bulky N-2 substituent that inhibits the enamine formation and competes with the benzyl group for the stereocontrol of the process.[31]

The photoaminocatalyst **3c** was found not reactive in the photoredox process. This can be attributed to the presence of bulky trityl groups. The trityl pyrrolidine was introduced by Maruoka as effective organocatalyst.[32] The use of trityl pyrrolidine have been reported in enamine[33] and iminium[34,23] catalysis. One of us has recently reported the practical and straightforward synthesis of protected *anti* 2-alkoxy-3-trityl-pyrrolidins from the commercial available (*R*)-3-hydroxypyrrolidinehydrochloride.[23] Although the bulky trityl group can block the approach of the electrophile to enamine, such as the $Ar_2COSiMe_3$ group of the classical and commercially available Hayashi-Jørgensen catalyst,[35] Mayr pointed out the subtle stereoelectronic effect played by the trityl substituents.[36] He reported that negative hyperconjugative interaction of the trityl group with the lone pair of the enamine nitrogen determines a reduction of the nucleophilicity of the enamine. As a consequence of the electronic effect, the trityl group in the 2-position of the pyrrolidine increases the electrophilic reactivity of iminium ions derived from unsaturated aldehydes.

An alternative explanation for the lack of reactivity of **3c** is the different Brønsted basicity. Recently, Mayr has reported Brønsted basicities pK_{aH} (i.e., pK_a of the conjugate acids) of pyrrolidines and imidazolidinones, as well as their nucleophilicities, determined by kinetic investigation of the reactions with benzhydrylium ions (Ar_2CH^+) and structurally related quinones. Among all the pyrrolidines studied, pyrrolidines bearing in □-position the trityl group were found the less nucleophilic ones.[37] However, all the mentioned studies were related to interaction of polar groups (electrophiles) with the enamine.

It is well known that the photoredox stereoselective alkylation of aldehydes is a radical process.[38] As malonyl radical is involved in our process, we have carried out some investigation of the reactivity of enamines with malonyl radical, in order to shed some light on the factors that could determine the catalysts' activity. We conducted a series of preliminary DFT calculations, using the unrestricted Becke-Half-and-Half-LYP functional[39] (uBHandHLYP/6-31g(d)//uBHandHLYP/cc-pvtz in DMF).

In particular, we modelled the addition pathways of the dimethyl-malonate radical (**7**) to the enamines (**8b**,**c**) derived from propanal with simplified catalysts, in which the photoactive side-chain of **3b** and **3c** had been replaced by an hydrogen and by a benzyl group, respectively (Figure 4). The first simplified catalyst is the 1st generation MacMillan catalyst (**2d**),[40] while the second had already been tested as an efficient organocatalyst in the enantioselective Michael addition of malonates to α,β-unsaturated aldehydes.[23]

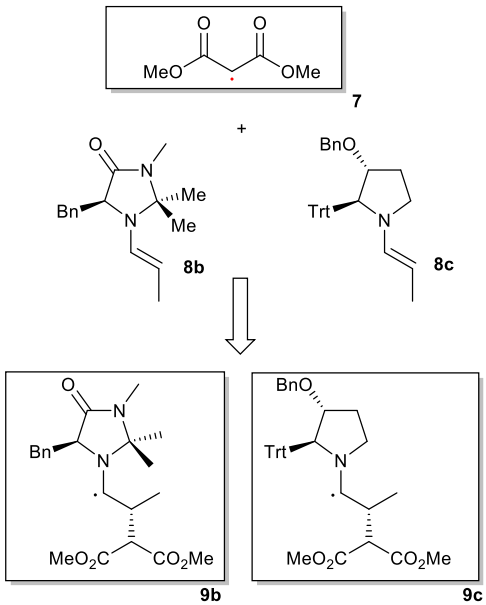

Fig. 4. Structures of the reagents and products analyzed in DFT calculations.

The energy profiles relative to the addition of malonate radical to enamines **8b** and **8c** (Figure 5) resulted very similar, both in the gas-phase and using DMF as the solvent, clearly excluding a contribution of the radical addition step in determining the lack of reactivity of the trityl-derived catalysts.

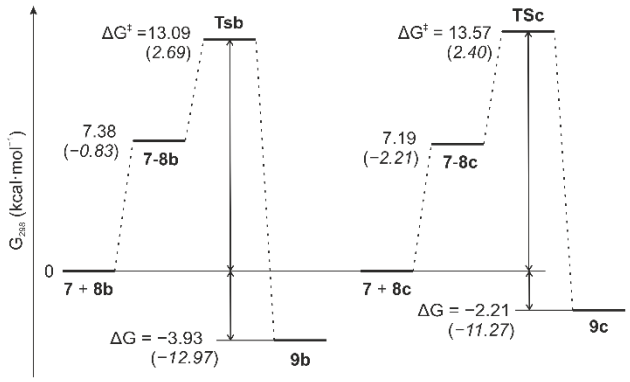

Fig. 5. Free energy profile (kcal·mol^{-1}) for the addition of dimethylmalonate radical (**7**) to enamine **8b** (left) and **8c** (right) in the gas-phase at the uBHandHLYP/6-31G(d) level of theory. Energies in parentheses are relative to single point calculations at the uBHandHLYP/cc-pvtz level of theory in DMF. Optimized structures and computational details are reported in the Supporting Information.

The lack of reactivity showed by the hybrid catalyst **3c** could be more related to the stereo-electronic properties of the substituted pyrrolidine. In a recent article, Wennemers and co-workers highlighted the importance of the pyramidalization direction of the enamine nitrogen in the reactivity of chiral enamine derived from cyclic amines.[41] Cyclic amines with different ring sizes revealed that *endo*-pyramidalized enamines are significantly more reactive compared to *exo*-pyramidalized analogs. The latter reacts slower due to the steric hindrance between the incoming electrophile and the substituent present in the □-position. If the enamine derived from **3c** is maintaining the *endo*-pyramidalization, the presence of the substituent in β-position can diminish the efficiency of the radical attack. Finally, given the long alkyl linker between the photoredox centre and the organocatalyst in **3c**, it is possible that the benefits from spatial proximity in this bifunctional catalyst are very limited, which might lead to its low reactivity.

The major finding of our investigation relies in the remarkable reactivity observed with the supramolecular photo-organocatalyst formed with the first generation of MacMillan imidazolidinone catalyst. It is important to mention that the effective catalyst used in alkylation of aldehydes is the catalyst **2e** depicted in Figure 1.[11] The same catalyst was used in different processes mediated by different photocatalysts.[12,15,16] It is also worth adding that, although these processes appear very similar, the photoredox mechanism involved is very different. When $[Ru(bpy)_3]^{2+}$ was employed by MacMillan as photocatalyst[11] the process is occurring via a reductive quenching forming $[Ru(bpy)_3]^{+}$, able to reduce the bromomalonate and forming the malonyl radical. In other processes[12,15] an oxidative quenching of the photocatalyst by the bromomalonate is operative. However, in the mentioned examples the effective organocatalyst, capable of forming the chiral enamine responsible for the stereoselective transformation, is **2e**. Other imidazolidinone catalysts, and in particular the first generation of imidazolidinones was proven to be less reactive and selective in the same reaction conditions. Unfortunately, the catalyst **2e** is not quite stable and its *cis* form gives worse results than *trans* form.[42] Remarkably, the first generation of catalysts (**2d**) were found effective in the enantioselective α-benzylation of aldehydes,[43] based on the mechanistic principle of spin-center shift recently reported by MacMillan, using alcohols as alkylating agents.[44] In this work, the catalyst **2e** was found ineffective. In some photoredox reactions, it was reported that the aminal in the C2 position on the imidazolidinone framework was susceptible to H-atom abstraction, leading to a decreased efficiency of the catalyst due to this decomposition pathways.[45] The first generation of imidazolidinone catalyst appears more robust and less prone to such decompositions.

In order to get further insight on the reaction mechanism, quenching experiments were performed. Upon addition of each reaction components (at the same concentration used in the optimized reaction conditions) to a DMF solution of complex **3b**, no quenching of the photocatalyst phosphorescence was observed (see SI for more details).

Since the photophysical behaviour of the complex **3b** is not affected by the reagents, the role of the enamine transiently formed on the photocatalyst was then examined. Enamine derived from phenylacetaldehyde and **3b** catalyst was chosen for these studies due to its stability versus hydrolysis. The enamine can be generated *in situ* adding an excess of phenylacetaldehyde to a **3b** solution in presence of triflic acid or can be separately prepared and isolated. In the first case, after 24 hours from the addition of phenylacetaldehyde to a **3b** solution in the presence of triflic acid, the emission decay of the solution showed two lifetime components of 102 and 8.3 ns (Figure 6). The long component is attributed to the unreacted **3b** photocatalyst by the close similarity of the lifetime (110 ns, Figure 6). The short component is attributed to the intramolecular quenching of the Ir complex ($[Ir]^{+}$) by the formed enamine with a quenching constant of 1.1×10^{8} s^{-1} and a quenching efficiency as high as 92%.

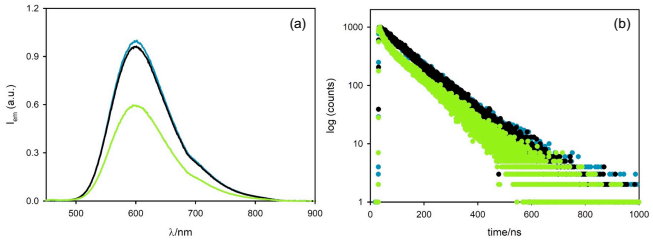

Fig. 6. Emission spectra (a) and emission intensity decays (b) of **3b** (1.70 x 10^{-4} M) and equimolar triflic acid in air-equilibrated DMF solution (blue line (a); blue dots (b)), right after the addition of phenylacetaldehyde 0.045 M (black line (a); black dots (b)) and after one day (green line(a); and green dots (b)). Optical pathlength 1 cm; λ_{exc} = 405 nm.

The enamine was also prepared and isolated, but due to the presence of both the iridium photocatalytic moiety and the reactive enamine, the product was not stable enough to be fully characterized (see SI for details). In any case, photophysical analysis performed using the freshly isolated enamine, showed similar results to the ones obtained with *in situ* prepared enamine (Figure S8).

On the basis of the photophysical evidences, a reaction mechanism is proposed and illustrated in Scheme 2.

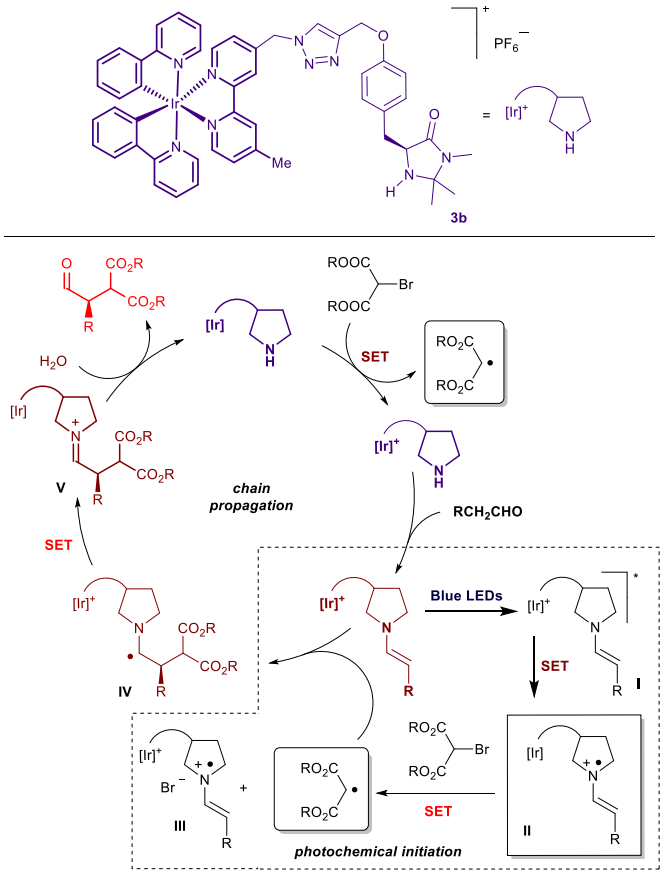

Scheme 2. Suggested mechanism for the enantioselective alkylation of aldehyde reaction with the linked iridium-MacMillan catalyst **3b**.

Upon excitation of the Ir complex, a reductive quenching takes place: the process is thermodynamically allowed, based on the excited state reduction potential of the Ir(III) photosensitiser of +0.95 V vs SCE (see SI for more details) and an estimated potential for enamine oxidation of +0.85 V vs SCE.[46] The process results in the formation of the reduced photosensitiser (**II**, Scheme 2), a strong reductant able to generate the alkyl radical from bromoderivative. This event starts the photoredox cycle as suggested by MacMillan.[11] We have no evidence about the fate of the sacrificial enamine after its oxidation (**III**, Scheme 2), namely if it could be restored to an effective catalyst. Concerning the on-cycle □-ammino radical (**IV**, Scheme 2), this species could engage a SET with bromoderivative to re-generate the alkyl radical, or an inter- or intramolecular SET with the iridium complex to form the corresponding iminium ion (**V**, Scheme 2). In the latter cases the reduced iridium complex formed was capable of the generation of the alkyl radical. Probably, as demonstrated by Yoon, the reaction is a radical chain but we do not have enough evidences to sustain this hypothesis.[38] However, in our reaction irradiation with visible light is mandatory.

Conclusions

In this study, we designed and characterized a supramolecular system composed of an Ir(III) photosensitizer and a MacMillan organocatalyst and we preliminary investigated its reactivity and selectivity in the benchmark alkylation reaction aliphatic aldehydes. Mechanistic photophysical studies demonstrated a fast and very efficient (92%) intramolecular reductive quenching of the iridium photosensitizer by enamine. The reduced iridium catalyst is able to form, from bromo-derivatives, alkyl electron poor radicals, involved in the reaction with chiral enamines to perform the enantioselective □-alkylation of aldehydes. Moreover, the bifunctional organo-photocatalyst **3b** proved to be considerably more efficient and selective as compared to the catalytic system formed by mixing the single separated components. Differently from previous investigations, the typical MacMillan *trans* catalyst used in many transformations is avoided, and a simple and more stable organocatalyst can be employed. The conjugation of the organocatalyst allow a design that could be further implemented and could allow the immobilization of this type of catalyst for flow applications. Future studies will be aimed also at the replacement of the phosphorescent iridium photosensitizer with fluorescent organic dyes. Indeed, the supramolecular approach relieves the constraint of the long-lived excited state by taking advantage of the close proximity of the photosensitizer and organocatalyst which results in a fast and efficient intramolecular quenching process.

Conflicts of interest

There are no conflicts to declare.

Acknowledgements

National PRIN 2017 projects (ID: 20174SYJAF, SURSUMCAT and ID: 20172M3K5N, CHIRALAB) are acknowledged for financial support of this research.

Notes and references

1 For selected reviews on photoredox catalysis, see: a) K. Zeitler, *Angew. Chem. Int. Ed.*, 2009, **48**, 9785-9789; *Angew. Chem.*, 2009, **121**, 9969-9974; b) T. P. Yoon, M. A. Ischay and J. Du, *Nat. Chem.*, 2010, **2**, 527-532; c) J. M. R. Narayanam and C. R. J. Stephenson, *Chem. Soc. Rev.*, 2011, **40**, 102-113; d) F. Teplý, *Collect. Czech. Chem. Commun.*, 2011, **76**, 859-917; e) J. Xuan and W. Xiao, *Angew. Chem.*, 2012, **124**, 6934-6944; *Angew. Chem. Int. Ed.*, 2012, **51**, 6828-6838; f) L. Shi and W.-J. Xia, *Chem. Soc. Rev.*, 2012, **41**, 7687-7697; g) D. Ravelli and M. Fagnoni, *ChemCatChem*, 2012, **4**, 169-171; h) Y. Xi, H. Yi and A. Lei, *Org. Biomol. Chem.*, 2013, **11**, 2387-2403; i) R. A. Angnes, Z. Li, C. R. D. Correia and G. B. Hammond, *Org. Biomol. Chem.*, 2015, **13**, 9152-9167; j) K. L. Skubi, T. R. Blum. and T. P. Yoon, *Chem. Rev.*, 2016, **116**, 10035-10074; k) X. Lang, J. Zhao and X. Chen, *Chem. Soc. Rev.*, 2016, **45**, 3026-3038; l) M. Parasram and V. Gevorgyan, *Chem. Soc. Rev.*, 2017, **46**, 6227-6240; m) K. N. Lee and M.-Y. Ngai, *Chem. Commun.*, 2017, **53**, 13093-13112; n) Y. – Q. Zou, F. M. Hoermann and T. Bach, *Chem. Soc. Rev.*, 2018, **47**, 278-290; o) L. Marzo, S. K. Pagire, O. Reiser and B. König, *Agew. Chem.*, 2018, **130**, 10188-10228; *Angew. Chem. Int. Ed.*, 2018, **57**, 10034-10072; q) S. P. Pitre, C. D. McTiernan and J. C. Scaiano, *Acc. Chem. Res.*, 2016, **49**, 1320−1330.
2 C. K. Prier, D. A. Rankic and D. W. C. MacMillan, *Chem. Rev.*, 2013, **113**, 5322-5363.
3 R. C. McAtee, E. J. McClein and C. R. J. Stephenson, *Trends in Chem.*, 2019, **1**, 111-125.
4 A. Studer and D. P. Curran, *Angew. Chem.*, 2015, **128**, 58-106; *Angew. Chem. Int. Ed.*, 2015, **55**, 58-102.
5 C. Chatgilialoglu and A. Studer, *Encyclopedia of Radicals in Chemistry, Biology and Materials*, Vol. 1–4, Wiley, Chichester, UK, 2012.
6 F. O'Hara, D. G. Blackmond and P. S. Baran, *J. Am. Chem. Soc.*, 2013, **135**, 12122-12134.
7 J. M. Smith, S. J. Haworth and P. S. Baran, *Acc. Chem. Res.*, 2018, **51**, 1807-1817.
8 A. Juris, V. Balzani, F. Barigelletti, S. Campagna, P. Belser and A. Von Zelewsky, *Coord. Chem. Rev.*, 1988, **84**, 85–277.
9 a) C. B. Kelly, N. R. Patel, D. N. Primer, M. Jouffroy, J. C. Tellis and G. A. Molander, *Nat. Protoc.*, 2017, **12**, 472-492; b) M.-A. Tehfe, M. Lepeltier, F. Dumur, D. Gigmes, J.-P. Fouassier and J. Lalevée, *Macromol. Chem. Phys.*, 2017, **218**, 1700192.
10 V. Balzani, P. Ceroni and A. Juris *Photochemistry and Photophysics: Concepts, Research, Applications*, Wiley, Chichester, UK, 2014.
11 D. A. Nicewicz and D. W. C. MacMillan, *Science*, 2008, **322**, 77-80.
12 A. Gualandi M. Marchini, L. Mengozzi, H. Tesfay Kidanu, A. Franc, P. Ceroni and P. G. Cozzi, *Eur. J. Org. Chem.*, 2020, 1486-1490.
13 A. E. Allen and D. W. C. MacMillan, *Chem. Sci.*, 2012, **3**, 633-658.
14 A. N. Alba, M. Viciano and R. Rios, *ChemCatChem*, 2009, **1**, 437-439.
15 A. Gualandi, M. Marchini, L. Mengozzi, M. Natali, M. Lucarini, P. Ceroni and P. G. Cozzi, *ACS Catal.*, 2015, **5**, 5927-5931.
16 a) M. Cherevatskaya, M. Neumann, S. Füldner, C. Harlander, S. Kümmel, S. Dankesreiter, A. Pfitzner, K. Zeitler and B. König, *Angew. Chem.*, 2012, **124**, 4138-4142; *Angew. Chem. Int. Ed.*, 2012, **51**, 4062-4066; b) P. Riente, A. Mata

Adams, J. Albero, E. Palomares and M. A. Pericàs, *Angew. Chem.*, 2014, **126**, 9767-9770; *Angew. Chem. Int. Ed.*, 2014, **53**, 9613-9616.
17 M. Neumann, S. Füldner, B. König and K. Zeitler, *Angew. Chem.*, 2009, **123**, 981-985; *Angew. Chem. Int. Ed.*, 2011, **50**, 951-954.
18 A. Bahamonde and P. Melchiorre, *J. Am. Chem. Soc.*, 2016, **138**, 8019-8030.
19 H. Mayr, S. Lakhdar, B. Maji and A. R. Ofial, *Beilst. J. Org. Chem.*, 2012, **8**, 1458-1478.
20 S. Lakhdar, B. Maji and H. Mayr, *Angew. Chem.*, 2012, **124**, 5837-5840; *Angew. Chem. Int. Ed.*, 2012, **51**, 4739-4742.
21 G. Lelais and D. W.C. MacMillan, *Aldrichimica Acta*, 2006, **39**, 79-87.
22 T. Rigotti, A. Casado-Sánchez, S. Cabrera,R. Pérez-Ruiz M. Liras, V. A. de la Peña O 'Shea and J. Alemán, *ACS Catal.*, 2018, **8**, 5928−5940.
23 C. Rosso, M. G. Emma, A. Martinelli, M. Lombardo, A. Quintavalla, C. Trombini, Z. Syrgiannis and M. Prato, *Adv. Synth. Catal.*, 2019, **361**, 2936–2944.
24 Z. Xun, T. Yu, Y. Zeng, J. Chen, X. Zhang, G. Yang and Y. Li, *J. Mater. Chem. A*, 2015, **3**,12965−12971.
25 T, Mede, M, Jäger and U. S. Schubert, *Chem. Soc. Rev*., 2018, **47**, 7577−7627.
26 S. Pagoti, D. Dutta and J. Dasha, *Adv. Synth. Catal.*, 2013, **355**, 3532–3538.
27 a) K. Du, C. Lu, Z. Chen, J. Nie and G. Yang, *Catal. Lett.*, 2016, **146**, 1107–1112; b) J. Y. Ying, J. Lim, S. S. Lee and S. N. B. Riduan, 2008, WO 2008/115154 A1.
28 J. Xie, M. Rudolph, F. Rominger and A. S. K. Hashmi, *Angew. Chem. Int. Ed.*, 2017, **56**, 7266-7270.
29 J. D. Slinker, A. A. Gorodetsky, M. S. Lowry, J. Wang, S. Parker, R. Rohl, S. Bernhard and G. G. Malliaras, *J. Am. Chem. Soc.*, 2004, **126**, 2763-2767.
30 M. Silvi, E. Arceo, I. D. Jurberg, C. Cassani and P. Melchiorre, *J. Am. Chem. Soc.*, 2015, **137**, 6120-6123.
31 A. M. P. Salvo, F. Giacalone, R. Noto and M. Gruttadauria, *ChemPlusChem*, 2014, **79**, 857-862.
32 T. Kano, H. Mii and K. Maruoka, *J. Am. Chem. Soc.*, 2009, **131**, 3450–3451.
33 M. Shimogaki, H. Maruyama,S. Tsuji, C. Homma, T. Kano and K. Maruoka, *J. Org. Chem.*, 2017, **82**, 12928–12932.
34 T. Kano, H. Maruyama, C. Homma and K. Maruoka, *Chem. Commun.*, 2018, **54**, 176–179.
35 B. S. Donslund, T. K. Johansen, P. H. Poulsen, K. S. Halskov and K. A. Jørgensen, *Angew. Chem.*, 2015, **127**, 14066-14081; *Angew. Chem. Int. Ed.*, 2015, **47**, 13860-13874.
36 H. Erdmann, F. An, P. Mayer, A. R. Ofial, S. Lakhdar and H. Mayr, *J. Am. Chem. Soc.*, 2014, **136**, 14263-14269.
37 F. An, B. Maji, E. Min, A. R. Ofial and H. Mayr, *J. Am. Chem. Soc.*, 2020, **142**, 1526-1547.
38 M. A. Cismesia and T. P. Yoon, *Chem. Sci.*, 2015, **6**, 5426-5434.
39 A. D. Becke, *J. Chem. Phys.*, 1993, **98**, 5648−5652.
40 E. Anniinä, M. Inkeri and P. M. Petri, *Chem. Rev.*, 2007, **107**, 5416–5470.
41 T. Schnitzer, J. S. Möhler and H. Wennemers, *Chem. Sci.*, 2020, **11**, 1943-1947.
42 D. A. Nagib, M. E. Scott and D. W. C. MacMillan, *J. Am. Chem. Soc.*, 2009, **131**, 10875-10877.
43 H.-W. Shih , M. N. Vander Wal , R. L. Grange and D. W. C. MacMillan, *J. Am. Chem. Soc.*, 2010, **132**, 13600-13603.
44 E. D. Nacsa and D. W. C. MacMillan, *J. Am. Chem. Soc.*, 2018, **140**, 3322-3330.
45 G. Cecere, C. M. König, J. L. Alleva and D. W. C. MacMillan, *J. Am. Chem. Soc.*, 2013, **135**, 11521-11524.
46 The calculated oxidation potential of (*E*)-enamine derived from the condensation of (5*R*)-2,2,3-trimethyl-5-benzyl-4-imidazolidinone with propanal. is +0.85 V (vs SCE); see: Y. Li, D. Wang, L. Zhang and S. Luo, *J. Org. Chem.*, 2019, **84**, 12071-12090.